AIAA JOURNAL
Vol. 53, No. 2, February 2015

Innovative Discrete-Vortex Model for Dynamic Stall Simulations

Enrico G. A. Antonini,* Gabriele Bedon,† Stefano De Betta,‡ Luca Michelini,§
Marco Raciti Castelli,¶ and Ernesto Benini**
University of Padua, 35131 Padova, Italy

DOI: 10.2514/1.J053430

An innovative model based on the vortex theory is presented with the aim of simulating the two-dimensional airfoil dynamic behavior at pitching reduced frequencies related to vertical axis wind-turbine operative conditions. The model relies on the introduction of a second separated wake from the suction side to correctly account for the aerodynamic effects of stall conditions and is provided with correction models whose aim is to consider the dynamic evolution of the shed vortices and of the separation point. The model receives as input experimental data to estimate the nonoscillating steady-state separation point for different angles of attack. A validation procedure confirmed the model capabilities to provide reliable numerical estimations of the lift coefficient for a pitching airfoil compared to experimental tests and computational-fluid-dynamics approaches based on the unsteady Reynolds-averaged Navier–Stokes equations complemented with the k-ω shear-stress transport turbulence model. In particular, the dynamic stall phenomenon is correctly simulated, providing lift coefficients in a hysteresis cycle. In addition, the computational effort is strongly reduced compared to the other computational tools and therefore enables the model to be used in routines with several simulation calls (e.g., optimization).

Nomenclature

a_1	=	Squire's parameter
$a_{i,j}$	=	influence coefficient, 1/m
C_l	=	lift coefficient
c	=	airfoil chord, m
c_f	=	circulation reduction factor
dl	=	integration length, m
$\boldsymbol{e}$	=	unit vector
f	=	pitching frequency, Hz
k	=	reduced pitching frequency
N	=	number of airfoil panels
n	=	integer determining the flow velocity shape
$\boldsymbol{n}_i$	=	panel normal unit vector
Re	=	Reynolds number
Re_v	=	vortex Reynolds number
RHS	=	right-hand side for the influence velocity equation system, m/s
r_c	=	vortex core radius, m
r_{c_0}	=	initial vortex core radius, m
$\boldsymbol{r}_i$, r_i	=	distance from the ith vortex center to the point where the induced velocity is computed, m
t	=	time, s
V_∞	=	freestream wind speed, m/s
$\boldsymbol{V}$, V	=	velocity vector and norm, m/s
$\boldsymbol{V}_b$, V_b	=	velocity vector and norm induced by an airfoil lumped vortex, m/s
$\boldsymbol{V}_i$, V_i	=	velocity vector and norm induced by a generic lumped vortex, m/s
$\boldsymbol{V}_l$, V_l	=	downstream velocity vector and norm with respect to the shear layer, m/s
$\boldsymbol{V}_r$, V_r	=	velocity vector and norm due to the motion of the panel, m/s
$\boldsymbol{V}_s$, V_s	=	velocity vector and norm induced by a wake lumped vortex shed from the separation point, m/s
$\boldsymbol{V}_{\text{tot},i}$, $V_{\text{tot},i}$	=	total velocity vector and norm induced on the ith panel element, m/s
$\boldsymbol{V}_{\text{tot},j}$, $V_{\text{tot},j}$	=	total velocity vector and norm induced on the jth wake element, m/s
$\boldsymbol{V}_u$, V_u	=	upstream velocity vector and norm with respect to the shear layer, m/s
$\boldsymbol{V}_w$, V_w	=	velocity vector and norm induced by a wake lumped vortex shed from the trailing edge, m/s
x_{dy}	=	dynamic separation point
x_{st}	=	nonoscillating steady-state separation point
y^+	=	nondimensional distance, based on local cell fluid velocity, from the wall to the first mesh node
α	=	airfoil angle of attack, deg
α_L	=	Oseen parameter
$\boldsymbol{\Gamma}_b$, Γ_b	=	total airfoil lumped vortex intensity vector and norm, m^2/s
$\boldsymbol{\Gamma}_{b,i}$, $\Gamma_{b,i}$	=	airfoil panel lumped vortex intensity vector and norm, m^2/s
$\boldsymbol{\Gamma}_i$, Γ_i	=	generic lumped vortex intensity vector and norm, m^2/s
$\boldsymbol{\Gamma}_s$, Γ_s	=	separated wake lumped vortex intensity vector and norm, m^2/s
$\boldsymbol{\Gamma}_w$, Γ_w	=	trailing-edge wake lumped vortex intensity vector and norm, m^2/s
Δt	=	time step, s
Δx, Δy	=	vortex element displacements, m
ν	=	kinematic viscosity, m^2/s
τ	=	time constant, s

Received 25 February 2014; revision received 8 August 2014; accepted for publication 11 August 2014; published online 26 November 2014.

*Research Engineer, Department of Industrial Engineering, Via Venezia 1; enricogiuseppeagostino.antonini@studenti.unipd.it.

†Ph.D. Student, Department of Industrial Engineering, Via Venezia 1; gabriele.bedon@dii.unipd.it.

‡Research Engineer, Department of Industrial Engineering, Via Venezia 1; stefano.debetta@studenti.unipd.it.

§Research Engineer, Department of Industrial Engineering, Via Venezia 1; luca.michelini@studenti.unipd.it.

¶Research Associate, Department of Industrial Engineering, Via Venezia 1; marco.raciticastelli@unipd.it.

**Associate Professor, Department of Industrial Engineering, Via Venezia 1; ernesto.benini@unipd.it.

I. Introduction

THE simulation with numerical models of the aerodynamic behavior of an oscillating airfoil is largely debated in the literature. A general analytical theory for the prediction of the dynamic effects of separated flows is still not developed [1,2], and to obtain reliable data, experimental tests and computational fluid dynamics (CFD) simulations are still mandatory. The objective of this work is to derive and prove the validity of an enhanced two-

dimensional discrete-vortex model to predict the dynamic behavior of a symmetrical airfoil.

Common approaches for the numerical simulation of two-dimensional airfoil aerodynamics rely on the panel method, which, in the basic formulation, provides good estimations limited to attached flow conditions. Alternatively, thin symmetrical profiles can be represented by a number of concentrated vortices placed along a limited straight line, where the no-penetration condition is imposed on discrete points. This method is widely used for airplane wing aerodynamics simulations, and an extensive discussion can be found in Katz and Plotkin [3]. The prediction of the poststall behavior is, however, still not included in the basic formulation.

Several attempts have been conducted to extend the previously described methods to a wider range of angles of attack. Jones [4] studied the case of the unsteady separated flow of an inviscid fluid around a moving flat plate with the introduction of a leading-edge vortex and developed a fast numerical algorithm to compare his results with experimental data. The work highlighted an increased aerodynamic normal force and torque in the unsteady conditions with respect to the steady case. This model was further extended by other authors [5,6] who considered different experimental data and different vortex models. A more general approach considers a second separated vortex shed from the airfoil suction side at a determined separation point provided from experimental tests or estimated by means of viscous boundary-layer computations. This methodology was implemented in the panel method by Oler et al. [7]. The authors, however, highlighted a computational inaccuracy for the non-oscillating steady-state conditions, linked to the incomplete and inaccurate modeling of the viscous/inviscid interactions in the immediate vicinity of the separation point [7]. A good agreement for the lift and drag coefficients was obtained by Katz [8,9], including an additional separated wake in a nonviscous vortex code; the intensity of the wake vorticity was computed as a result from the resultant flowfield velocity, and the shedding point was included as an input obtained from experimental tests. Ramesh et al. [10] recently presented a new criterion for intermittent vortex shedding from a rounded leading edge to be adopted in discrete-vortex methods. The use of a single empirical parameter, linked to the maximum allowable leading-edge suction, allowed to determine the onset, growth, and termination of leading-edge vortices. Good agreement is found with experimental and numerical results with respect to forces and complex flows.

Stationary and unsteady separations have been also studied considering the Navier–Stokes equations, in particular focusing on the leading edge and on the generated eddy structures due to Rayleigh instabilities. Osswald et al. [11] implemented a fully implicit direct-numerical-simulation methodology for an unsteady analysis considering a velocity–vorticity formulation to simplify the theoretical and numerical analysis of maneuvering flight. The rapid pitch-up of a NACA 0015 airfoil is examined at $Re = 1000$ and $Re = 10,000$, identifying a possible sequence of events depicting the basic mechanism responsible for the evolution and subsequent shedding of the dynamic stall vortex. Bhaskaran and Rothmayer [12] studied the two-dimensional, unsteady, leading-edge flow over stationary, pitching, and oscillating airfoils using the Navier–Stokes equations for flow past a parabola. They showed that the eddy creation before reversal in the base flow generally agrees with the theory of Rayleigh instabilities, with a wavelength in reasonable agreement with the theoretical value. Morris and Rusak [13] investigated the inception of leading-edge stall on stationary, two-dimensional, smooth, thin airfoils at low to moderately high Reynolds number flow by a reduced-order, multiscale model problem via numerical simulations. The study reveals the fundamental nature of leading-edge stall on a stationary airfoil. It is found that there exists a limit approximately equal to 300 on the modified Reynolds number. When the value is below this limit, the flow is dominated by the increasing effect of the adverse pressure gradient, which eventually overcomes the viscous stresses ability to keep the boundary layer attached to the airfoil. However, when the value increases above the limit value, the unsteady convective structures relax the effect of the adverse pressure gradient on the viscous boundary layer to delay the onset of stall in the mean flow with respect to marginal separation theory results [14,15].

In the present work, a discrete-vortex model including a separated wake is considered and improved with additional numerical models to take into account the airfoil dynamic stall behavior. The model is designed to be adopted for the simulation of the blade profile of a Darrieus vertical axis wind turbine and to enable the optimization of its shape. The particular operative conditions are comparable to a pitching airfoil with a specific range of reduced frequencies, for which the validation will be focused. To simulate the airfoil dynamic behavior due to the change in the angle of attack that leads to different aerodynamic loads on the blade, additional models need to be considered. Several vortex models that describe the temporal development of the vortices have been developed in the past [16]. The model proposed by Vatistas et al. [17] is adopted in the present work because of its simple formulation and reasonable accuracy when dealing with concentrated vortices. This model allows the introduction of a core radius, whose growth behavior can be expressed as suggested by Bhagwat and Leishman [18]. In addition to the vortex models, the influence of the airfoil dynamic behavior must be considered for the estimation of the separation point. Experimental data of nonoscillating steady-state separation points for different Reynolds numbers are not widely available in literature, whereas different methods for their estimation are quite common [19]; most of them refer to iterative procedures. In the present formulation, a simple model based on the lift on a flat plate in a potential Kirchhoff flow, described by Thwaites [20], is considered, and the results are corrected to provide a better agreement with the experimental data. To account for the delay in the shift of the dynamic separation point, an empirical formulation is adopted, which is inspired by the time-dependent correlations introduced in the Beddoes–Leishmann dynamic stall model for the angle of attack [21].

The proposed vortex model is particularly suitable for moderately thin profiles, and therefore the NACA 0012 was selected as a case study. The obtained results are compared with both CFD simulations and experimental data. The CFD analyses, based on a validated simulation of a pitching airfoil, were conducted using the commercial software ANSYS Fluent 14. Several experimental data are available in literature for the NACA 0012 profile; the first results for dynamic stall were presented by McCroskey et al. [22,23] and McAlister et al. [24]. However, Gerontakos [25] provided aerodynamic coefficients both for the steady and for the unsteady cases with the same testing conditions, enabling the model validation in both cases.

II. Vortex Model

The proposed work is based on a discrete-vortex scheme, where the airfoil is approximated into a series of flat plate elements, each of them represented by a single lumped vortex located at the center of pressure of the element itself (i.e., at the quarter-chord, according to the flat plate theory). In the present model, a number of flat elements equal to eight is considered; the assumption will be confirmed to be reasonable, as shown in the nonoscillating steady-state condition validation. The boundary condition of zero normal flow for each flat plate element is imposed, which means that the airfoil is considered as a streamline:

$$\boldsymbol{V}_{\text{tot},i} \cdot \boldsymbol{n}_i = 0 \tag{1}$$

where $\boldsymbol{V}_{\text{tot},i}$ and $\boldsymbol{n}_i$ are the air velocity vector for the ith panel and the unit normal vector, respectively. The normal velocity is computed at the three-quarter-chord of each element to fulfill the Kutta condition at the airfoil trailing edge [3].

The influence of the lumped vortex in any point of the flowfield is computed by

$$\boldsymbol{V}_i = \frac{\Gamma_i}{2\pi r_i}\boldsymbol{e} \tag{2}$$

where Γ_i is the vortex strength, r_i is the distance from the vortex center to the point where the induced velocity is computed, and $\boldsymbol{e}$ is the unit vector in the direction of $\boldsymbol{r}_i \times \boldsymbol{\Gamma}_i$.

To simulate an unsteady flow, a shedding wake is added to this scheme; the airfoil's circulation changes in time, and the discrete-vortex wake elements are shed from the trailing edge at every time step. The wake and the airfoil circulation must fulfill Kelvin's law, which imposes the total circulation generated in the flow to be zero:

$$\frac{\mathrm{D}\Gamma}{\mathrm{D}t} = 0 \tag{3}$$

The model can be extended to separated flows around airfoils at high angles of attack introducing a shear layer that is emitted from a separation point in the suction side of the airfoil, as proposed by Katz [8] and shown in Fig. 1a, at a fixed distance normal to the airfoil chord. The adopted distance is obtained through the validation with nonoscillating steady-state condition data, as explained next. The chordwise coordinate of the separation point (which is a function of Reynolds number, airfoil type, and angle of attack) and the strength of the separated wake vortex are evaluated considering the following semi-empirical model.

The intensity of the vortex shed at the separation point can be estimated considering a line integral enclosing part of the shear wake just behind the separation point itself [8], as can be seen in Fig. 1b, which yields

$$\frac{\mathrm{d}\Gamma_s}{\mathrm{d}t} = \frac{\mathrm{d}}{\mathrm{d}t}\oint \boldsymbol{V}\cdot \mathrm{d}\boldsymbol{l} = \frac{1}{2}(V_u^2 - V_l^2) \tag{4}$$

where Γ_s is the circulation strength generated at the separation point, $\boldsymbol{V}$ is the velocity vector, $d\boldsymbol{l}$ is the integration length, V_u is the upstream wind speed with respect to the shear layer, and V_l is the downstream wind speed. A circulation reduction factor c_f is introduced (because not all the vorticity generated in the boundary layer is injected in the flowfield at the separation point), whose value is set to 0.6, as proposed by Katz [8]. The strength of the latest separated wake element is therefore

$$\Gamma_s = \frac{c_f}{2}(V_u^2 - V_l^2)\Delta t \tag{5}$$

On the basis of a weighted average of the the experimental results obtained from Fage and Johansen [26], the authors suggest for the present model a constant upper velocity of $V_u = 1.4V_\infty$ and a constant lower one of $V_l = 0$, leading to a constant value for the strength of the latest vortex shed at the separation point and therefore neglecting minor fluctuations.

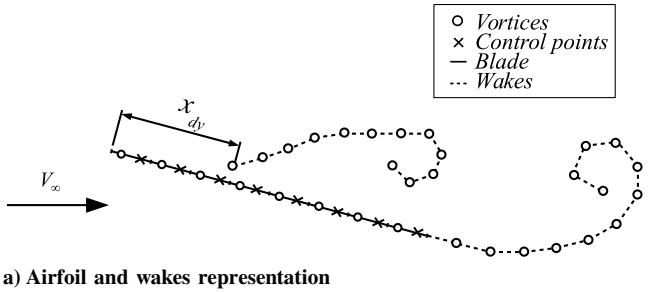

a) Airfoil and wakes representation

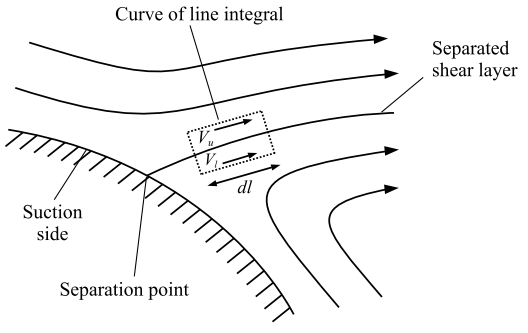

b) Integration path on the separation line

Fig. 1 Schematic description of the adopted model [8].

The position of the separation point is first estimated as if the lift on the airfoil was generated by a flat plate in a potential Kirchhoff flow [20]:

$$x_{st} = \left(2\sqrt{\frac{C_l}{C_{l,\alpha}\cdot\alpha}} - 1\right)^2 \tag{6}$$

where C_l is the nonoscillating steady-state lift coefficient, and $C_{l,\alpha}$ is the linear lift slope. The nonoscillating steady-state lift coefficients provided by experimental data for a fixed Reynolds number of $1.35\cdot 10^5$ and for the NACA 0012 airfoil are considered in the present work. The separation point coordinates are afterward slightly adjusted to fit the computed nonoscillating steady-state lift coefficients with the database values. The normal distance of the latest shed vortex from the airfoil chord is then investigated; the position of this vortex is of crucial importance because it can lead to numerical problems in the computation of the induced velocities, if placed on the chord line or very close to it, or to incorrect physical description of the problem, if placed at large distances. Within this range, different normal distances are investigated, namely $0.03c$, $0.05c$, $0.07c$, and $0.09c$. The authors observed that, for distances of $0.03c$, $0.07c$, and $0.09c$, the lift coefficient estimation is not reliable for the considered range of angles of attack (between 0 and 25 deg). On the other hand, a normal distance equal to $0.05c$ ensures the algorithm convergence and provides values similar to the flat plate case; such distance is therefore assumed for the proposed computations. The evolution of the lift coefficient as a function of the angle of attack and the comparison between the estimated (flat plate) separation points and the corrected ones are shown in Fig. 2.

The generation of the circulation due to the separated flow has to be taken into account to fulfill Kelvin's law:

$$\frac{\mathrm{D}\Gamma}{\mathrm{D}t} = \Gamma_b(t) - \Gamma_b(t-\Delta t) + \Gamma_w + \Gamma_s = 0 \tag{7}$$

where Γ_b is the total bound circulation of the airfoil, Γ_w is the strength of the latest vortex shed at the trailing edge, and Γ_s is the strength of the latest vortex shed at the separation point.

To correctly reproduce the effect of the dynamic stall, a delay in the movement of the boundary-layer separation point needs to be considered, as reported by Hansen et al. [21]. An estimation of the dynamic separation point can be obtained from the nonoscillating steady-state separation one:

$$x_{dy}(t+\Delta t) = x_{st} + (x_{dy}(t) - x_{st})e^{(\Delta t/\tau)} \tag{8}$$

where x_{st} and x_{dy} are the separation point for steady and unsteady conditions, respectively, and τ is the time constant, which in this model is set to $4c/V_\infty$, as suggested by Hansen et al. [21].

A viscous vortex model, which allows to avoid singularity conditions in the induced velocity calculation and to reproduce the vortex decay in time, is additionally included. This is particularly necessary in a vertical-axis wind-turbine rotor simulation, where the blades and the wakes collide and interfere at different times due to the rotor circular motion. The hereby adopted model was first proposed by Vatistas et al. [17], obtaining good agreement with experimental results. The swirl-velocity profile generated by an infinite straight vortex becomes

$$\boldsymbol{V}_i = \frac{\Gamma_i}{2\pi}\left(\frac{r_i}{(r_c^{2n} + r_i^{2n})^{(1/n)}}\right)\boldsymbol{e} \tag{9}$$

where r_c is the vortex core radius, and n is an integer determining the flow velocity shape. In this work, n was assumed equal to 2, leading to a close approximation of the Lamb–Oseen model, which provides a good approximation of the experimental results [27,28]. The vortex core radius is modeled as a time-dependent solution, with the vortex viscosity included to take into account the effects of vortex growth and initial finite vortex core [29]:

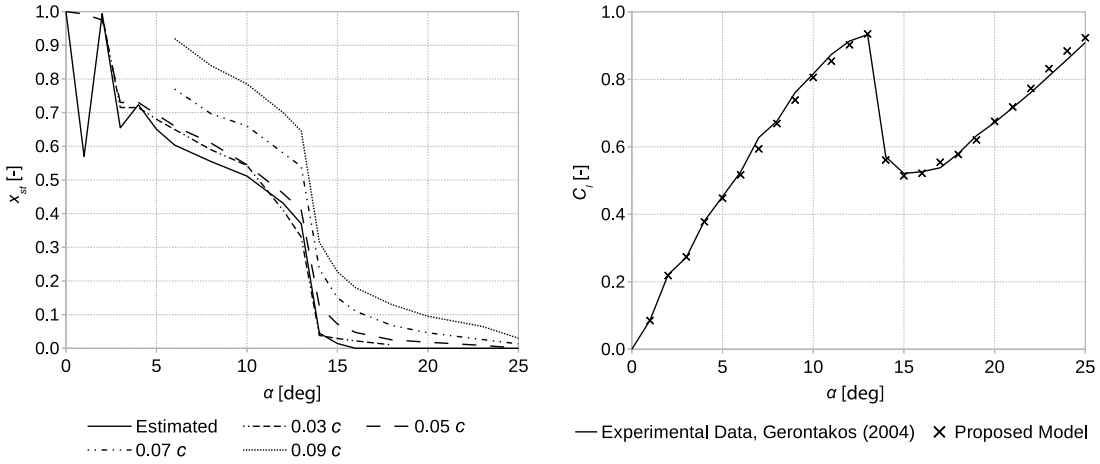

a) Estimated vs corrected separation points as a function of the normal distance of the separation point from the chord line

b) Non-oscillating steady state results

Fig. 2 Nonoscillating steady-state validation of the vortex model, NACA 0012 at $Re = 1.35 \cdot 10^5$.

$$r_c(t) = \sqrt{r_{c_0} + 4\alpha_L \nu (1 + a_1 Re_v)t} \tag{10}$$

where r_{c_0} is the initial vortex core radius, set to $0.10c$ as proposed by Bhagwat and Leishman [18]; α_L is the Oseen parameter [30], equal to 1.25643; ν is the kinematic viscosity; a_1 is Squire's parameter set to $2 \cdot 10^4$, according to the experimental measurements performed by Bhagwat and Leishman [28], which describes adequately the vortex core growth; and Re_v is the vortex Reynolds number ($Re_v = \Gamma_v/\nu$).

Some remarks have to be made on the Kutta condition for unsteady flows. Very high oscillating frequencies, large amplitudes, and high angles of attack may cause trailing-edge separation, thus violating the Kutta condition. This situation was investigated with experimental studies by Archibald [31] and Poling and Telionis [32] concluding that, even though the Kutta condition is no more valid, the variations in both lift and pressure distribution can be neglected.

The model is solved for successive time steps considering one equation for Kelvin's law [Eq. (7)] and N equations for the no-penetration boundary condition:

$$\boldsymbol{V}_{\text{tot},i} \cdot \boldsymbol{n}_i = (\boldsymbol{V}_\infty + \boldsymbol{V}_b + \boldsymbol{V}_w + \boldsymbol{V}_s - \boldsymbol{V}_r)_i \cdot \boldsymbol{n}_i = 0 \tag{11}$$

where $\boldsymbol{V}_b$, $\boldsymbol{V}_w$, and $\boldsymbol{V}_s$ are the foil, wake, and separated wake-induced velocities, respectively, and $\boldsymbol{V}_r$ is the velocity due to the motion of the ith panel. The $N + 1$ unknowns are the circulation strengths of the N panels and of the most recent element in the trailing-edge wake, whereas the remaining vortex intensities in the trailing-edge wake and in the separated one are known.

Every induced velocity can be expressed as a linear combination of the vortex strength multiplied by an influence factor a. The system of equations takes the form

$$\begin{pmatrix} a_{1,1} & a_{1,2} & \dots & a_{1,N} & a_{1,W} \\ a_{2,1} & a_{2,2} & \dots & a_{2,N} & a_{2,W} \\ \vdots & \vdots & \ddots & \vdots & \vdots \\ a_{N,1} & a_{N,2} & \dots & a_{N,N} & a_{N,W} \\ 1 & 1 & \dots & 1 & 1 \end{pmatrix} \begin{pmatrix} \Gamma_1 \\ \Gamma_2 \\ \vdots \\ \Gamma_N \\ \Gamma_w \end{pmatrix} = \begin{pmatrix} \text{RHS}_1 \\ \text{RHS}_2 \\ \vdots \\ \text{RHS}_N \\ \Gamma_b(t - \Delta t) \end{pmatrix} \tag{12}$$

where RHS_i is the right-hand side, which includes the constant values induced by the wakes apart from the latest trailing-edge wake vortex. The airfoil circulation is then computed as the sum of the panels' circulation strength:

$$\Gamma_b(t) = \sum_{i=1}^{N} \Gamma_{b,i} \tag{13}$$

and the lift coefficient follows using the Kutta–Joukowski theorem:

$$C_l = \frac{2\Gamma_b}{V_\infty c} \tag{14}$$

The drag coefficient is not considered because the viscous analysis of the airfoil boundary layer is still not modeled; the drag force estimation would be therefore not reliable in the whole operative range.

Each vortex moves downstream with the local absolute velocity because vortex wakes are force-free. In each time step, the vortex element displacements are calculated by

$$(\Delta x, \Delta y)_j = \boldsymbol{V}_{\text{tot},j} \cdot \Delta t \tag{15}$$

The latest vortex element of both trailing and separated wakes is placed at half of the distance traveled by the airfoil during one time step to obtain an efficient wake discretization [9].

The choice of the time step, as suggested by Katz [8], must fulfill the following boundaries to produce good results:

$$0.05 < \frac{\Delta t V_\infty}{c} < 0.2 \tag{16}$$

A value of 0.1 is chosen in the present model.

III. Experimental Data

The experimental data provided by Gerontakos [25] are used in the present work as reference values; the experiment was conducted in a subsonic wind tunnel with a cross-section area of 120×90 cm^2 and a length of 270 cm. A sinusoidally oscillating airfoil (equipped with two tip plates of 30 cm diameter to avoid three-dimensional flows due to the tip effects) was considered, and its aerodynamics was investigated at $Re = 1.35 \cdot 10^5$ by means of closely spaced multiple hot-film sensor arrays supplemented by surface pressure measurements, hot-wire wake velocity surveys, and smoke-flow visualizations. The gaps between the oscillatory airfoil and the stationary tip plates were kept within 1 mm to minimize the leakage of the blade-tip flow [33]. These aspects allow therefore to assume the flow to be two-dimensional and suitable for this study. Pitching reduced frequencies between 0.025 and 0.100 were investigated:

$$k = \frac{\pi f c}{V_\infty} \tag{17}$$

where f is the pitching frequency, c is the airfoil chord, and V_∞ is the unperturbed freestream wind speed. The angle of attack varies with the following law:

$$\alpha = 10 + 10\ \sin(2\pi f t) \tag{18}$$

where t is the time.

The sinusoidal motion of the airfoil at the considered reduced frequencies are closely related to the operating conditions in the blade airfoil of a Darrieus turbine [33], and therefore the validation on these experimental data is considered reliable.

IV. Computational-Fluid-Dynamics Analysis

To accurately reproduce the flow over the pitching NACA 0012 airfoil, a full campaign of two-dimensional CFD analyses based on the unsteady Reynolds-averaged Navier–Stokes (URANS) equations is performed. As shown in Fig. 3, the fluid domain is subdivided into two regions: a circular rotating inner zone enclosing the airfoil and embedded within a stationary outer zone (covering the whole external computational domain and characterized by a circular opening, centred on the airfoil aerodynamic centre). The inlet is located at $30c$ upwind from the airfoil center of pressure, and a velocity inlet boundary condition is imposed, with a velocity of 14 m/s and a gauge pressure of 0 Pa. The turbulence conditions were specified through the turbulence intensity and the viscosity ratio parameters, which are set to 0.08% and 10 respectively [33]. The outlet is located at $60c$ downwind from the airfoil center of pressure, and a pressure outlet boundary condition is imposed, with a gauge pressure of 0 Pa. These boundary conditions are placed far enough to obtain an uniform freestream velocity before the airfoil [33] and to allow the full development of the wake. The side boundaries of the domain are set to symmetry and located at $30c$ from the airfoil center of pressure to avoid blockage effects. No roughness was considered along the airfoil surface.

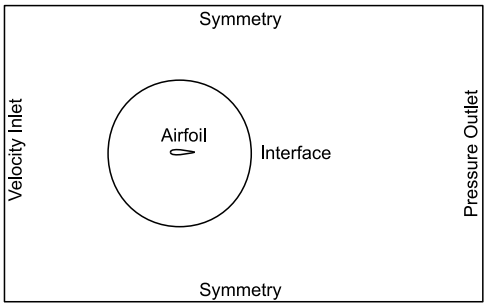

Fig. 3 Boundary conditions of the computational domain.

Table 1 Average error in lift coefficient estimation for different turbulence models, $k = 0.025$

Model	Average error, %
k-ϵ standard	5.40
k-ϵ realizable	7.54
k-ω standard	5.02
k-ω SST	2.29
Spalart–Allmaras	3.63

Figure 4 shows some details of the adopted hybrid structured/unstructured mesh; 225 nodes are placed on both the pressure and the suction sides of the airfoil, at a distance of $3.31 \cdot 10^{-4}c$ from the walls, to obtain a y^+ close to 1. The structured grid is composed of 40 rows clustered around the airfoil surface with a growth rate of 1.05.

The nonlinear governing equations for the conservation of mass, momentum, and turbulence are solved by the commercial software ANSYS Fluent 14, which is based on a finite-volume method. A coupled scheme with a second-order spatial discretization is adopted, with the absolute residuals set to 10^{-5}, because lower orders would not lead to significant solution variations. The pitching motion of the airfoil (and of the circular rotating inner grid) is imposed by means of a user-defined function. The time step is computed to obtain a value of the Courant number below 0.15 [34] at the interface between the rotational and the stationary domains. The independence of the solution from the mesh size was obtained with successive refinements until almost identical results near the airfoil and in the wake region were registered.

To correctly predict the flow around the pitching airfoil, several turbulence models are considered: k-ϵ standard, k-ϵ realizable, k-ω standard, k-ω shear-stress transport (SST), and Spalart–Allmaras [35]. The enhanced wall treatment is considered for the k-ϵ models. The average error in the lift coefficient estimation for the different models is reported in Table 1. The k-ω SST model is chosen due to its lowest average error compared to the experimental data for a reduced pitching frequency of $k = 0.025$. In fact, as can be clearly seen in Fig. 5, the other models fail to predict both the deep stall zone of the curve and the downstroke phase of the hysteresis cycle because of the inability to simulate flows with large separation regions and severe adverse pressure gradients [33].

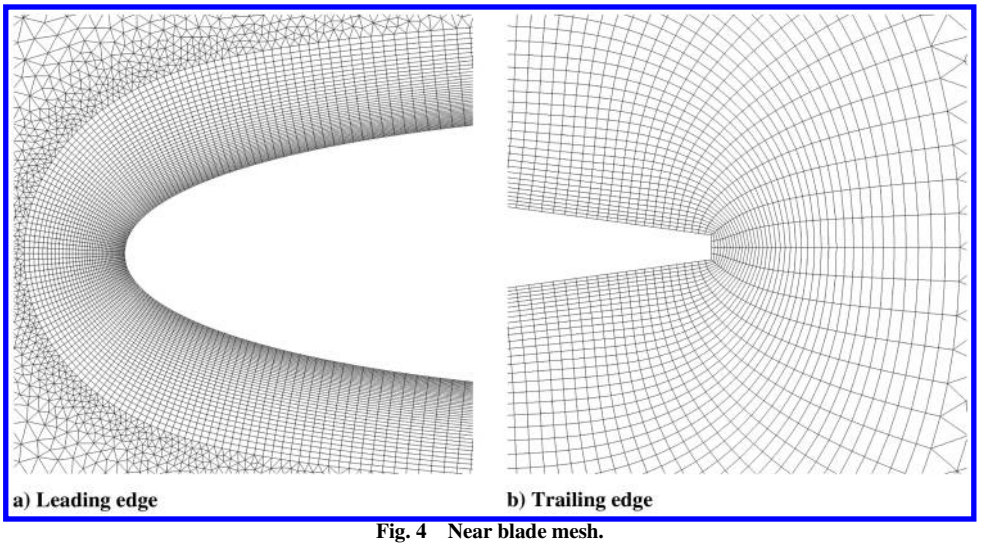

Fig. 4 Near blade mesh.

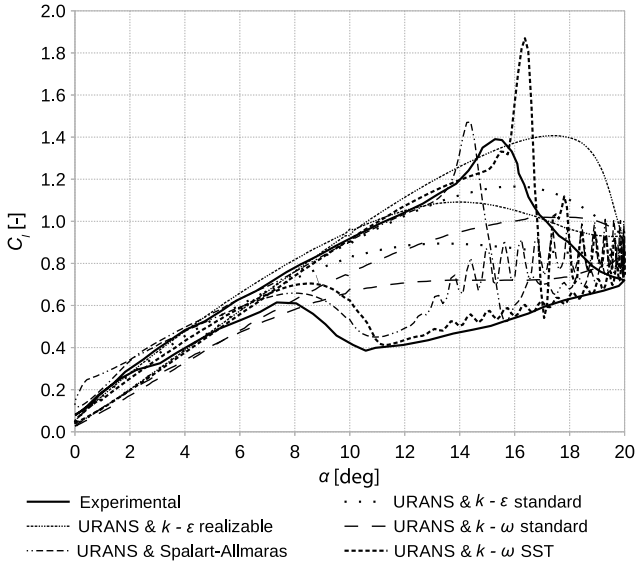

Fig. 5 URANS validation, NACA 0012 at $Re = 1.35 \cdot 10^5$, $k = 0.025$.

V. Simulation Results

The lift coefficient estimations from the proposed vortex model for the pitching NACA 0012 airfoil are shown in Fig. 6 as well as the experimental data from Gerontakos [25] and the results of the CFD simulations for different pitching reduced frequencies.

For increasing angles of attack (from 0 deg to approximately 14 deg), the lift coefficient and the curve slope provided by the vortex code are reliable but slightly underestimated with respect to both the CFD and the experimental data for pitching reduced frequencies of $k = 0.025$ and $k = 0.050$. The results obtained for the highest pitching frequency ($k = 0.100$) are instead superimposed to the experimental one.

For angles of attack between 15 and 20 deg (i.e., where the experimental lift coefficient reaches the maximum value), the CFD code clearly overpredicts the lift coefficient, whereas the vortex model is more conservative. The CFD overprediction is linked to the sharp lift coefficient dropoff after the stall, which brings to a bad prediction of the flow reattachment in the downstroke phase, as observed also by Wang et al. [36] for the transition SST model. The CFD result is also characterized by high oscillations linked to the two-dimensional simulation, as observed by Wang et al. [33] and Martinat et al. [37]. The vortex model provides a lift coefficient curve very close to the average values from CFD. The model, however, provides an underestimation of the peak lift coefficient, linked to an overestimation of the vortex intensity in the separated wake.

A great reduction in the overall computational time is achieved using the proposed model (1 h against more than 24 h required by the CFD calculations on a desktop computer equipped with an Intel i7-870 CPU and 16 GB RAM).

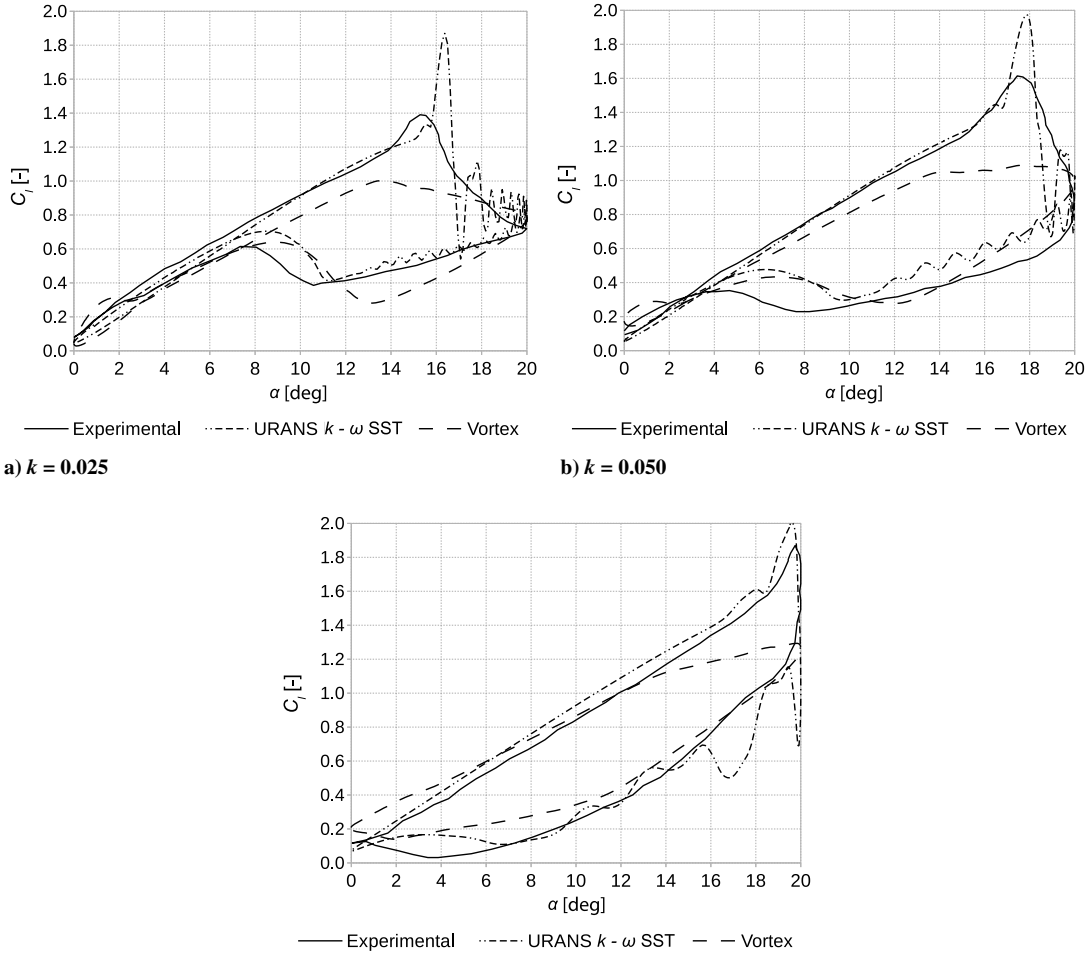

a) $k = 0.025$ **b) $k = 0.050$**

c) $k = 0.100$

Fig. 6 Comparison between experimental, URANS k-ω SST, and vortex results for different pitching reduced frequencies, NACA 0012 at $Re = 1.35 \cdot 10^5$.

VI. Conclusions

A vortex model is presented, which includes a separated wake to simulate the deep stall behavior and dynamic models for both the separation point and the vortex intensity evolution. Good results are obtained in the nonoscillating steady-state case, and the model capabilities in predicting the dynamic stall are investigated.

The predicted hysteresis in the lift coefficient is compared to both experimental data and CFD simulations. The most reliable results are obtained for the highest pitching frequency ($k = 0.100$), whereas a lower accuracy is registered for the lower pitching frequencies ($k = 0.025$ and $k = 0.050$), where further investigation is required. CFD URANS k-ω SST simulations are also conducted for comparison with vortex. The results are reliable compared to experimental data except for the overestimation of the peak lift coefficient. A better agreement is again obtained for the highest pitching frequency.

A reliable estimation of the dynamic lift coefficient is achieved by the proposed model, especially for high airfoil pitching frequencies. The reduced computational requirements prompt for its adoption to provide aerodynamic data for unsteady computations and optimizations.

References

[1] Ericsson, L. E., and Reding, J. P., "Fluid Dynamics of Unsteady Separated Flow. Part 2. Lifting Surfaces," *Progress in Aerospace Sciences*, Vol. 24, No. 4, 1987, pp. 249–356. doi:10.1016/0376-0421(87)90001-7

[2] Holierhoek, J. G., de Vaal, J. B., van Zuijlen, A. H., and Bijl, H., "Comparing Different Dynamic Stall Models," *Wind Energy*, Vol. 16, No. 1, 2013, pp. 139–158. doi:10.1002/we.v16.1

[3] Katz, J., and Plotkin, A., *Low-Speed Aerodynamics*, Cambridge Univ. Press, Cambridge, England, U.K., 2001, pp. 264–272.

[4] Jones, M. A., "The Separated Flow of an Inviscid Fluid Around a Moving Flat Plate," *Journal of Fluid Mechanics*, Vol. 496, Dec. 2003, pp. 405–441. doi:10.1017/S0022112003006645

[5] Wang, C., and Eldredge, J. D., "Low-Order Phenomenological Modeling of Leading-Edge Vortex Formation," *Theoretical and Computational Fluid Dynamics*, Vol. 27, No. 5, 2013, pp. 577–598. doi:10.1007/s00162-012-0279-5

[6] Ramesh, K., Gopalarathnam, A., Edwards, J. R., Ol, M. V., and Granlund, K., "An Unsteady Airfoil Theory Applied to Pitching Motions Validated Against Experiment and Computation," *Theoretical and Computational Fluid Dynamics*, Vol. 27, No. 6, Jan. 2013, pp. 843–864. doi:10.1007/s00162-012-0292-8

[7] Oler, J. W., Strickland, J. H., Im, B. J., and Graham, G. H., "Dynamic Stall Regulation of the Darrieus Turbine," Sandia National Lab. Rept. SAND83-7029, Albuquerque, NM, 1983.

[8] Katz, J., "A Discrete Vortex Method for the Non-Steady Separated Flow over an Airfoil," *Journal of Fluid Mechanics*, Vol. 102, No. 1, 1981, pp. 315–328. doi:10.1017/S0022112081002668

[9] Katz, J., "Large-Scale Vortex-Lattice Model for the Locally Separated Flow over Wings," *AIAA Journal*, Vol. 20, No. 12, 1982, pp. 1640–1646. doi:10.2514/3.7998

[10] Ramesh, K., Gopalarathnam, A., Granlund, K., Ol, M., and Edwards, J., "Discrete-Vortex Method with Novel Shedding Criterion for Unsteady Aerofoil Flows with Intermittent Leading-Edge Vortex Shedding," *Journal of Fluid Mechanics*, Vol. 751, June 2014, pp. 500–538. doi:10.1017/jfm.2014.297

[11] Osswald, G. A., Ghia, K. N., and Ghia, U., "Simulation of Dynamic Stall Phenomenon Using Unsteady Navier–Stokes Equations," *Computer Physics Communications*, Vol. 65, Nos. 1–3, 1991, pp. 209–218. doi:10.1016/0010-4655(91)90173-I

[12] Bhaskaran, R., and Rothmayer, A. P., "Separation and Instabilities in the Viscous Flow over Airfoil Leading Edges," *Computers & Fluids*, Vol. 27, No. 8, Nov. 1998, pp. 903–921.

[13] Morris, W. J., and Rusak, Z., "Stall Onset on Aerofoils at Low to Moderately High Reynolds Number Flows," *Journal of Fluid Mechanics*, Vol. 733, Sept. 2013, pp. 439–472. doi:10.1017/jfm.2013.440

[14] Stewartson, K., Smith, F. T., and Kaups, K., "Marginal Separation," *Studies in Applied Mathematics*, Vol. 67, No. 1, 1982, pp. 45–61.

[15] Ruban, A., "Asymptotic Theory of Short Separation Regions on the Leading Edge of a Slender Airfoil," *Fluid Dynamics*, Vol. 17, No. 1, 1982, pp. 33–41. doi:10.1007/BF01090696

[16] Saffman, P. G., *Vortex Dynamics*, Cambridge Monographs on Mechanics, Cambridge Univ. Press, Cambridge, England, U.K., 1995.

[17] Vatistas, G. H., Kozel, V., and Mih, W. C., "A Simpler Model for Concentrated Vortices," *Experiments in Fluids*, Vol. 11, No. 1, 1991, pp. 73–76. doi:10.1007/BF00198434

[18] Bhagwat, M. J., and Leishman, J. G., "Generalized Viscous Vortex Model for Application to Free-Vortex Wake and Aeroacoustic Calculations," *Proceedings of the 58th Annual Forum and Technology Display of the American Helicopter Society International*, Montreal, 2002.

[19] Cebeci, T., Mosinskis, G. J., and Smith, A. M. O., "Calculation of Separation Points in Incompressible Turbulent Flows," *Journal of Aircraft*, Vol. 9, No. 9, 1972, pp. 618–624. doi:10.2514/3.59049

[20] Thwaites, B., *Incompressible Aerodynamics: An Account of the Theory and Observation of the Steady Flow of Incompressible Fluid Past Aerofoils, Wings, and Other Bodies*, Dover, New York, 1960.

[21] Hansen, M. H., Gaunaa, M., and Madsen, H. A. R., "A Beddoes–Leishman Type Dynamic Stall Model in State-Space and Indicial Formulations," Risø National Lab. Rept. R-1354, Roskilde, Denmark, 2004.

[22] McCroskey, W. J., Carr, L. W., and McAlister, K. W., "Dynamic Stall Experiments on Oscillating Airfoils," *AIAA Journal*, Vol. 14, No. 1, 1976, pp. 57–63. doi:10.2514/3.61332

[23] McCroskey, W. J., McAlister, K. W., Carr, L. W., and Pucci, S. L., "An Experimental Study of Dynamic Stall on Advanced Airfoil Sections. Volume1. Summary of the Experiment," NASA TR-84245, 1982.

[24] McAlister, K. W., Carr, L. W., and McCroskey, W. J., "Dynamic Stall Experiments on the NACA 00i2 Airfoil," NASA TR-1100, 1978.

[25] Gerontakos, P., "An Experimental Investigation of Flow Over an Oscillating Airfoil," M.S. Thesis, McGill Univ., Montreal, 2004.

[26] Fage, A., and Johansen, F. C., "On the Flow of Air Behind an Inclined Flat Plate of Infinite Span," *Proceedings of the Royal Society of London. Series A, Containing Papers of a Mathematical and Physical Character*, Vol. 116, No. 773, 1927, pp. 170–197. doi:10.1098/rspa.1927.0130

[27] Coyne, A. J., Bhagwat, M. J., and Leishman, J. G., "Investigation into the Rollup and Diffusion of Rotor Tip Vortices Using Laser Doppler Velocimetry," *Proceedings of the 53rd Annual American Helicopter Society Forum*, Virginia Beach, VA, 1997.

[28] Bhagwat, M. J., and Leishman, J. G., "Measurements of Bound and Wake Circulation on a Helicopter Rotor," *Journal of Aircraft*, Vol. 37, No. 2, 2000, pp. 227–234. doi:10.2514/2.2611

[29] Squire, H. B., "The Growth of a Vortex in Turbulent Flow," *Aeronautical Quarterly*, Vol. 16, 1965, pp. 302–306.

[30] Oseen, C. W., "Über Wirbelbewegung in Einer Reibenden Flüssigkeit," *Arkiv för Matematik, Astronomi och Fysik*, Vol. 7, pp. 14–26, 1911.

[31] Archibald, F. S., "Unsteady Kutta Condition at High Values of the Reduced Frequency Parameter," *Journal of Aircraft*, Vol. 12, No. 6, 1975, pp. 545–550. doi:10.2514/3.44472

[32] Poling, D. R., and Telionis, D. P., "The Response of Airfoils to Periodic Disturbances—The Unsteady Kutta Condition," *AIAA Journal*, Vol. 24, No. 2, 1986, pp. 193–199. doi:10.2514/3.9244

[33] Wang, S., Ingham, D. B., Ma, L., Pourkashanian, M., and Tao, Z., "Numerical Investigations on Dynamic Stall of Low Reynolds Number Flow Around Oscillating Airfoils," *Computers & Fluids*, Vol. 39, No. 9, 2010, pp. 1529–1541. doi:10.1016/j.compfluid.2010.05.004

[34] Trivellato, F., and Raciti Castelli, M., "On the Courant–Friedrichs–Lewy Criterion of Rotating Grids in 2D Vertical-Axis Wind Turbine Analysis," *Renewable Energy*, Vol. 62, 2014, pp. 53–62. doi:10.1016/j.renene.2013.06.022

[35] "ANSYS Fluent 14.0 Theory Guide," ANSYS Inc., Canonsburg, PA, 2011.

[36] Wang, S., Ingham, D. B., Ma, L., Pourkashanian, M., and Tao, Z., "Turbulence Modeling of Deep Dynamic Stall at Relatively Low Reynolds Number," *Journal of Fluids and Structures*, Vol. 33, Aug. 2012, pp. 191–209. doi:10.1016/j.jfluidstructs.2012.04.011

[37] Martinat, G., Braza, M., Hoarau, Y., and Harran, G., "Turbulence Modelling of the Flow Past a Pitching NACA0012 Airfoil at 1e5 and 1e6 Reynolds Numbers," *Journal of Fluids and Structures*, Vol. 24, No. 8, 2008, pp. 1294–1303. doi:10.1016/j.jfluidstructs.2008.08.002

Z. Rusak
Associate Editor